Operating Characteristics of the P&O Algorithm at High Perturbation Frequencies for Standalone PV Systems

Mohammed A. Elgendy, Bashar Zahawi, *Senior Member, IEEE*, and David J. Atkinson

***Abstract*—The perturb and observe (P&O) algorithm is one of the most commonly utilized maximum power point tracking (MPPT) control schemes for photovoltaic (PV) generators. However, the operation of this algorithm at high perturbation frequencies, when the system response to MPPT perturbations is never allowed to settle, has not been given adequate attention in the literature. This paper characterizes system behavior in this mode of operation for standalone PV systems feeding resistive loads and motor-pump loads. Simulation and experimental results show that the P&O algorithm operating at a high perturbation frequency may offer higher energy utilization efficiency and better system performance, despite the resulting nonperiodic waveforms of the system.**

***Index Terms*—DC–DC power conversion, maximum power point tracking (MPPT), photovoltaic (PV) power systems, PV pumping.**

I. Introduction

A NUMBER of maximum power point tracking (MPPT) algorithms with different levels of complexity, efficiency, and implementation costs, have been proposed in the literature for standalone and grid-connected photovoltaic (PV) applications. Most of these algorithms have been comprehensively reviewed in a number of review papers [1]–[5]. The simplest and cheapest MPPT method maintains the PV array operation at a constant voltage [6] equal to its standard test conditions maximum power point (MPP) voltage provided by the manufacturer. At a small increase in implementation cost, the energy utilization efficiency can be significantly improved by employing the perturb and observe (P&O) MPPT technique. This is a simple algorithm that does not require previous knowledge of the PV generator characteristics or the measurement of solar intensity and cell temperature and is easy to implement with analog and digital circuits. The algorithm regularly perturbs the operating point of the PV generator by increasing or decreasing a control parameter by a small amount (step size) and measures the PV array output power before and after the perturbation. If the power increases, the algorithm continues to perturb the system in the same direction; otherwise, the system is perturbed in the opposite direction [7]–[21].

Three techniques have been proposed for implementing the P&O algorithm: reference voltage perturbation [7]–[14], reference current perturbation [15], [16], and direct duty ratio perturbation [8], [12], [17]–[19]. In reference voltage perturbation, the PV array output voltage reference is used as the control parameter in conjunction with a controller (usually a PI controller) to adjust the duty ratio of the MPPT converter. Similarly, the reference current perturbation approach uses the PV array output current reference as the control parameter. For direct duty ratio perturbation, the duty ratio of the MPPT converter is used directly as the control parameter.

Due to the continuous perturbations of the P&O algorithm, system waveforms fluctuate around their MPP values even if solar irradiance and cell temperature are constant. These usually fluctuate between three levels in the steady state when the perturbation frequency is low and the step size is high [8], [18]. The use of high step sizes results in high steady-state oscillations in the array voltage, decreasing the energy utilization efficiency of the system. The steady-state oscillations can be reduced by using lower step sizes. However, this slows down the starting transient of the MPPT algorithm as well as the response of the system to irradiance and temperature changes [7]–[10].

The slow transient response can be mitigated by using an adaptive step size scheme. This has already been investigated by many authors [9], [10], [12], [13], and [20]. However, adaptive step size schemes may require higher computational complexity and/or need system dependent constants [9]. The slow transient response can also be compensated for by using a higher perturbation rate. In this case, if the perturbation sampling period becomes shorter than the settling time of the system response, the system will never reach a steady state. The local stability of the system at the operating point can frequently be lost and the interaction between system dynamics and the MPPT perturbations results in irregular system waveforms. This may be the reason why most researchers to date have avoided operation in this mode.

The loss of local stability at the operating point does not necessarily mean that the system is globally unstable. With reference voltage perturbation and reference current perturbation, this loss of local stability may result in PI controller instability and thus loss of MPPT. However, with direct duty ratio

Manuscript received December 17, 2013; revised May 1, 2014; accepted June 11, 2014. Date of publication July 24, 2014; date of current version February 16, 2015. Paper no. TEC-00730-2013.

M. A. Elgendy is with the School of Electrical and Electronic Engineering, Newcastle University, Tyne and Wear NE1 7RU, U.K, and also with the New and Renewable Energy Department, Desert Research Center, Mataria, Cairo, Egypt (e-mail: mohammed.elgendy@ncl.ac.uk).

B. Zahawi is with the School of Electrical and Electronic Engineering, Newcastle University, Wear NE1 7RU, U.K., and also with the Department of Electrical and Computer Engineering, Khalifa University, Abu Dhabi, UAE (e-mail: bashar.zahawi@ncl.ac.uk).

D. J. Atkinson is with the School of Electrical and Electronic Engineering, Newcastle University, Wear NE1 7RU, U.K. (e-mail: dave.atkinson@ncl.ac.uk).

Color versions of one or more of the figures in this paper are available online at http://ieeexplore.ieee.org.

Digital Object Identifier 10.1109/TEC.2014.2331391

perturbation, global stability is maintained when higher perturbation rates up to the pulse-width modulation (PWM) rate or up to the analog to digital conversion (ADC) rate (if this is lower than the PWM rate) are used [8]. At high perturbation rates, although system waveforms are irregular and nonperiodic, they are always bounded by two levels and hence the system is globally stable.

When the P&O algorithm is employed in its conventional three-level operation mode, there is always a tradeoff between the magnitude of steady-state oscillations and the speed of the transient response. Even when the irradiance is constant, steady-state oscillations cannot be reduced beyond certain limits. This is because the use of very small step sizes (to reduce steady-state oscillations) will lead to algorithm confusion due to noise. When operated with high perturbation rates, however, the system will benefit from small steady-state oscillations and a fast transient response. The use of very small step sizes is not a significant problem in this case because even if the algorithm is confused due to noise, the perturbation direction would be corrected after a very short time.

This paper investigates the operating characteristics of the P&O algorithm when employed with the direct duty ratio perturbation technique at a high perturbation rate. Standalone PV systems with a resistive load and with a motor-pump load are considered in this study. The qualitative behavior of the systems is evaluated by numerical simulations and experimental results using a 1080-Wp PV installation. The quantitative behavior of the system is also assessed by calculating the energy utilization efficiency of the experimental system for different weather conditions. The results presented in this paper show that the algorithm may give better energy utilization when operated at high perturbation frequencies.

II. System Description

A PV system employing switching converters for MPPT control is a nonlinear time-varying system [8]. It comprises different sources of nonlinearity including the *I–V* characteristic of the PV generator, the switching action of the power electronic converter, the operation of the MPPT algorithm, and the characteristics of the nonlinear load (if any). Under constant and uniform irradiance and cell temperature conditions, the system should operate within a narrow interval around the MPP. It is then possible to develop a linearized analytical model to characterize system behavior around that equilibrium point. This can be accomplished by taking the averages of different variables over a switching cycle and linearizing any nonlinear function about the equilibrium point using Taylor's series. The Taylor series expansion of a nonlinear function $f(x)$ in the neighborhood of an operating point $(x = a)$ is given by

$$f(x) = \sum_{n=0}^{\infty} \frac{f^{(n)}(a)}{n!}(x-a)^n. \tag{1}$$

For the standalone PV system shown in Fig. 1, the Taylor series expansion can be applied to the nonlinear torque equation [6] of the motor-pump set to give the following linear relationship:

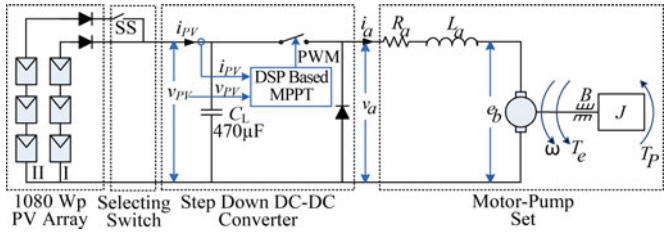

Fig. 1. Simplified circuit diagram of experimental PV pumping system.

$$T_e = k_1 + k_2\omega + J\frac{d\omega}{dt} \tag{2}$$

where k_1 and k_2 are constants that can be calculated from the Taylor series approximation of the summation of load and friction torques about the equilibrium point. At maximum power transfer, the PV generator can be replaced by a current source with parallel resistance R_{MPP} and the circuit can be modeled by [8]

$$\frac{dv_{\mathrm{PV}}}{dt} = \frac{2I_{\mathrm{MPP}}}{C_L} - \frac{1}{R_{\mathrm{MPP}}C_L}v_{\mathrm{PV}} - \frac{d}{C_L}i_a \tag{3}$$

$$\frac{di_a}{dt} = \frac{d}{L_a}v_{\mathrm{PV}} - \frac{R_a}{L_a}i_a - \frac{k}{L_a}\omega \tag{4}$$

$$\frac{d\omega}{dt} = \frac{k}{J}i_a - \frac{k_1}{J} - \frac{k_2}{J}\omega \tag{5}$$

where lower case symbols represent the quantities as function of time. Replacing each quantity by a dc term (represented by an upper case symbol) plus a small perturbation (represented by a lower case symbol with a circumflex), the small signal state space equations for the system are

$$\begin{pmatrix} \frac{d\hat{v}_{\mathrm{PV}}}{dt} \\ \frac{d\hat{i}_a}{dt} \\ \frac{d\hat{\omega}}{dt} \end{pmatrix} = \begin{pmatrix} \frac{-1}{R_{\mathrm{MPP}}C_L} & \frac{-D}{C_L} & 0 \\ \frac{D}{L_a} & \frac{-R_a}{L_a} & \frac{-k}{L_a} \\ 0 & \frac{k}{J} & \frac{-k_2}{J} \end{pmatrix} \begin{pmatrix} \hat{v}_{\mathrm{PV}} \\ \hat{i}_a \\ \hat{\omega} \end{pmatrix} + \begin{pmatrix} \frac{-I_a}{C_L} \\ \frac{V_{\mathrm{PV}}}{L_a} \\ 0 \end{pmatrix} \hat{d} \tag{6}$$

$$\hat{v}_{\mathrm{PV}} = \begin{pmatrix} 1 & 0 & 0 \end{pmatrix} \begin{pmatrix} \hat{v}_{\mathrm{PV}} & \hat{i}_a & \hat{\omega} \end{pmatrix}^T. \tag{7}$$

The aforementioned model can be solved analytically to predict the response of the system to a single MPPT perturbation, i.e., a small perturbation in duty ratio. At low perturbation rates, the sampling interval is long enough to allow the response to settle before the next perturbation is applied, resulting in a new equilibrium point. The analytical model can be used again for the next perturbation after updating the initial conditions

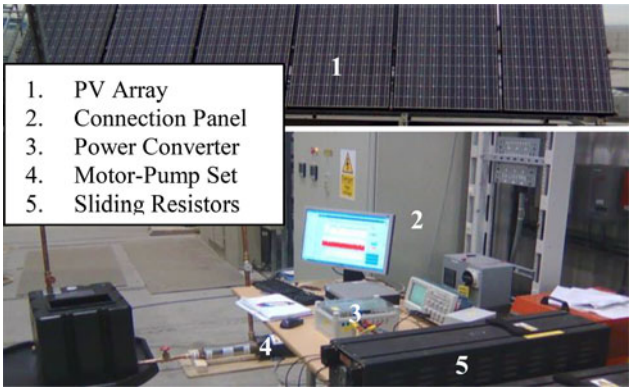

Fig. 2. Experimental PV pumping system.

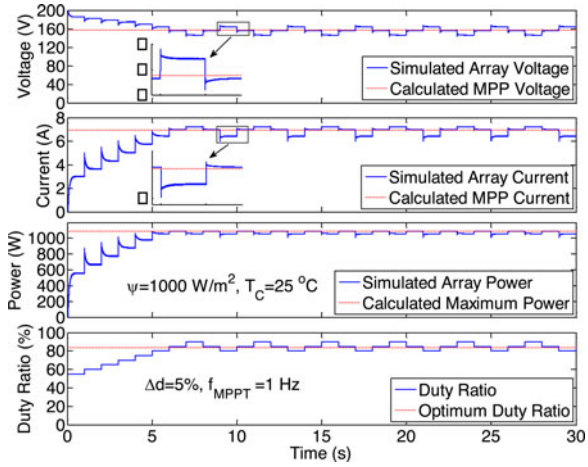

Fig. 3. Simulated system response under three-level operation.

and so on. A full derivation of the analytical solution and a comprehensive stability analysis of the system have already been presented by the authors in previous publications [8], [21].

At high perturbation rates, however, the sampling interval is very low and the system is never allowed to reach an equilibrium point and the linearized model is no longer valid. In this paper, system operation with a high perturbation rate is characterized based on experimental and simulation results. The numerical simulation of the system is developed using the measured characteristics of each individual component of the experimental system as described in [6]. The constructed experimental prototype comprised of six 180-Wp SANYO HIP-J54BE2 solar modules divided into two parallel branches of three series connected modules. The system also includes a step down dc–dc converter, a resistive load and a dc motor-pump load (see Fig. 2). A simplified circuit diagram of this system with the motor-pump load is shown in Fig. 1. For the resistive load, only one branch of the PV array is connected to avoid exceeding the current rating of the resistors. The measured characteristics of the PV array show slightly higher maximum power at lower MPP voltage than the nameplate values. The load resistance was fixed at 40 Ω and fed through a 2.2 mH–100 μF LC low-pass filter. The PV array current and voltage were measured with Hall effect sensors. For experimental flexibility and ease of programming, a Texas Instruments TMS320F2812 DSP based eZdsp kit was used for control and data acquisition. Meteorological parameters were recorded at a 1-s sampling rate utilizing a weather station installed on the same roof on which the PV array is installed. Motor armature resistance and inductance were measured at 1.25 Ω and 3.5 mH, respectively. The converter PWM switching frequency was fixed at 10 kHz, an appropriate choice for the IGBT switch used in the MPPT converter based on converter efficiency considerations. A link capacitance of 470 μF was employed, which is a commercially available size high enough to store generated energy during the off period of the converter switch with the required current ripple. At these parameter values, the converter operates in continuous current mode throughout the full range of duty ratio variations.

To study the starting and steady-state performance of the algorithm, the experimental system was initially run at constant solar intensity and cell temperature for 30 s, ignoring variations in solar irradiance within 1%. System parameters were recorded with a sampling rate of 2 K samples/s. A longer experimental test duration of 20 min was used to study the effects of weather variations on system behavior and to calculate the energy utilization efficiency for different weather conditions. In this test, parameters were recorded with a low acquisition rate of 10 samples/s to limit the host computer buffer size and the storage memory required for the acquisition files. Simulations were used to study the effects of the variations in step size and irradiance level on the behavior of the algorithm as these cannot be accomplished with a site installed PV array. Due to the similarity in system behavior with the two types of load, the discussion below will be limited to the motor-pump load except where stated otherwise.

III. System Waveforms

A PV system operating with P&O MPPT algorithm has two types of transients: one originates from variations in solar irradiance/cell temperature and the other from the perturbation of the tracking algorithm. Even under steady-state solar irradiance and temperature conditions, the system is still subjected to continuous step changes in duty ratio at the chosen perturbation frequency.

A. Time Waveforms

The continuous perturbations of the P&O algorithm result in steady-state fluctuations in system waveforms. At low perturbation rates, the sampling interval is long enough to allow the response to settle before the next perturbation. In this case, system response can be predicted using a linearized analytical model and the waveforms fluctuate between three levels around their MPP values as shown in Fig. 3. A detailed description of such an analytical model and system operation with three-level mode has been presented in [7], [8], and [18]. At high perturbation rates, the system is never allowed to reach a steady state. The P&O algorithm cannot distinguish between the power variations due to the perturbations and those resulting from system dynamics. The response to each individual MPPT perturbation

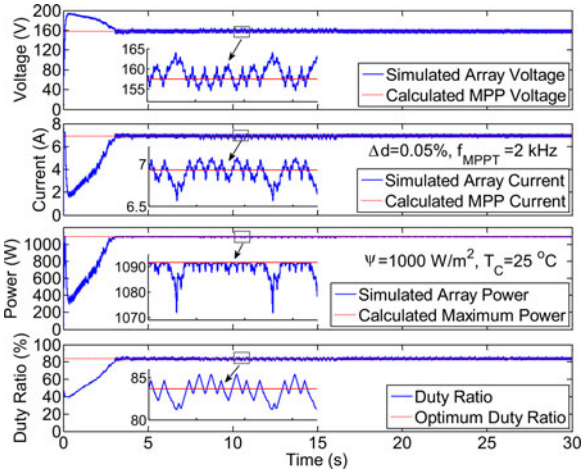

Fig. 4. Simulated system response at a high perturbation rate.

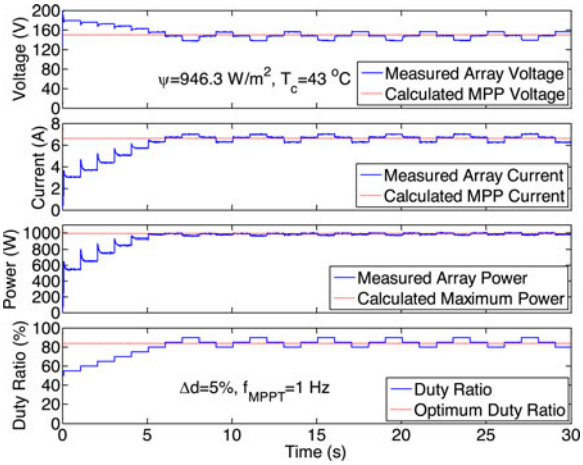

Fig. 5. Experimental system response under three-level operation.

depends on the conditions at the perturbation instant which vary continuously. The sensitivity of the system to initial conditions and the repeated confusion of the MPPT algorithm by system dynamics result in chaotic system behavior. As a result, the duty ratio and consequently the other parameters of the system oscillate around their MPP value in a chaotic manner.

Fig. 4 shows the chaotic array voltage, current, power and the duty ratio waveforms of the simulated system. These waveforms were obtained for operation at 1000 W/m^2 solar irradiance and 25 °C cell temperature with a perturbation rate of 2 kHz (the same as the ADC rate) and a step size of 0.05%. The duty ratio oscillates around its optimum value (83.61%) crossing the MPP forward and backward on each side of the MPP. At such a high perturbation rate and low step size, the P&O algorithm may easily be confused due to system dynamics and noise. The PV array voltage fluctuates around the MPP voltage (157.6 V) and the array current fluctuations around the MPP current (6.93 A) causing the array power to drop slightly below the maximum possible power (1091.6 W). Despite the local instability of the operating points, the waveforms of the system are always bounded by two levels hence the system is globally stable. Similar system waveforms are obtained from the experimental system for low perturbation rate operation (see Fig. 5) and high perturbation rate operation (see Fig. 6). The tests presented in these figures were carried out under different solar irradiance and cell temperature conditions since weather conditions cannot be controlled in a site PV installation.

To better understand the dynamic behavior of the P&O algorithm, a 0.05-s period of the power and duty ratio plots of Fig. 6 ($T = 14.2 - 14.25$ s) is magnified in Fig. 7. If the power is decreasing (periods A in Fig. 7), the P & o algorithm assumes that the power reduction is a result of the last MPPT perturbation and reverses the perturbation direction accordingly. Because of the slower response time of the motor-pump load (compared to the speed of the algorithm), the PV array output power may continue to decrease even after the direction of perturbation has been reversed. The algorithm will therefore be confused, reversing its perturbation direction forward and backward until

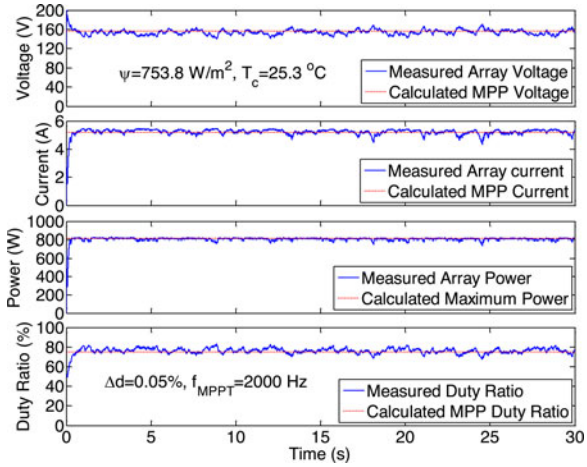

Fig. 6. Experimental system response at a high perturbation rate.

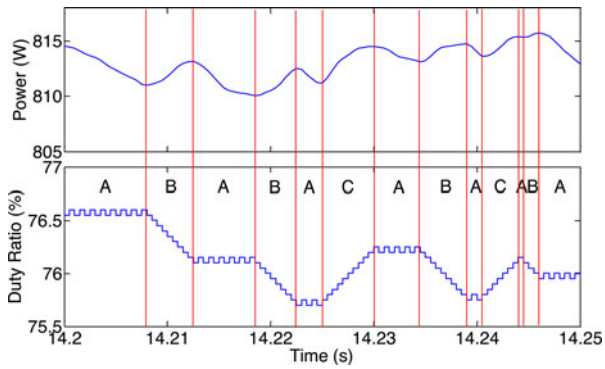

Fig. 7. Dynamic behavior of P&O algorithm at a high perturbation rate.

the power begins to increase (the end of the A periods). During periods B and C, the output power is increasing and the perturbation direction is maintained until the power begins to decrease. If the direction of perturbation just before the power increase was to decrease the duty ratio, the P&O algorithm continues to decrease it (periods B). If, however, the direction of perturbation

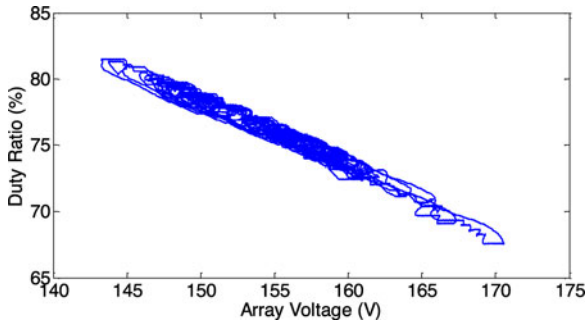

Fig. 8. Duty ratio-array voltage phase portrait.

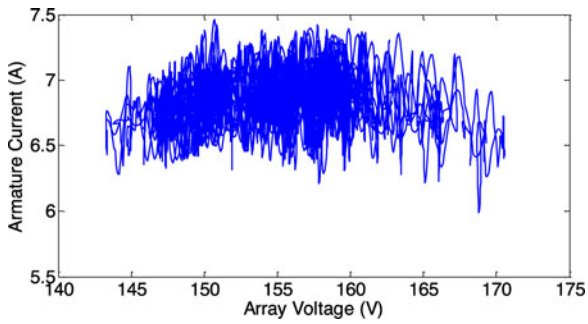

Fig. 9. Motor current-array voltage phase portrait.

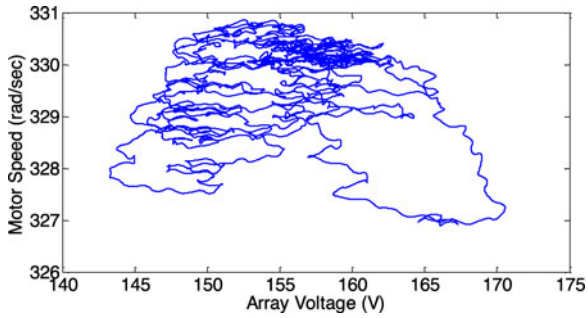

Fig. 10. Motor speed-array voltage phase portrait.

just before the power increase was to increase the duty ratio, the algorithm continues in the same direction (periods C).

Figs. 8–10 show three phase portraits of the experimental system waveforms shown in Fig. 6. All three phase portraits show bounded trajectories that never close onto themselves. These are typical responses for irregular, nonperiodic waveforms, but do not by themselves prove that the system is chaotic. In order to test whether the system is chaotic, its sensitivity to initial conditions is quantified by calculating the Lyapunov exponents [22]–[24] of system waveforms to identify whether nearby trajectories diverge or converge with time. For a system with n state space variables, Lyapunov spectrum consists of n average exponents ($\lambda_1\ \lambda_2 \ldots \lambda_n$) where λ_1 is the largest and λ_n is the smallest. If the sign of λ_1 is positive, this is normally sufficient for diagnosing chaos and local instability at the operating points [22]–[24].

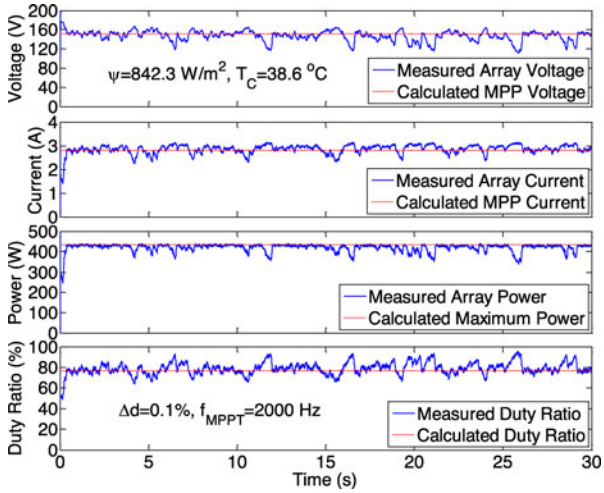

Fig. 11. Experimental system response under high perturbation rate; R-load.

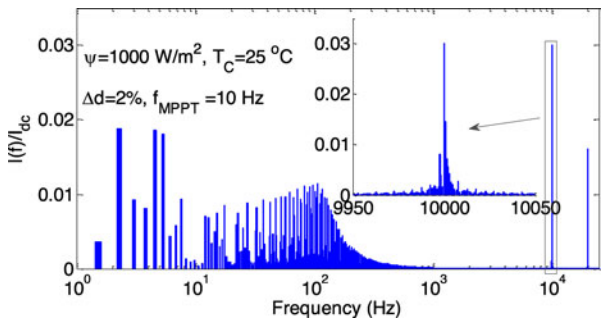

Fig. 12. Normalized frequency spectrum of motor current with three-level operation.

In this paper, λ_1 is calculated from the measured state variables of the system by utilizing Rosenstein's algorithm [25]. For the array voltage waveform (see Fig. 6), a segment of 20 000 samples of the steady-state part is examined by Rosenstein's algorithm. A positive largest Lyapunov exponent of about 3.7 is obtained indicating that the array voltage is chaotic. When motor current and speed waveforms were examined, λ_1 was calculated at 103 and 19.2, respectively.

Similar system waveforms were obtained with the resistive load when the P&O algorithm is employed with a high perturbation rate. Fig. 11 shows the waveforms of the experimental system at a perturbation rate of 2 kHz and a step size of 0.1%. As shown, system waveforms oscillate around the MPP values in chaotic patterns. Again, despite the local instability of the operating points, the system waveforms are bounded hence the system is globally stable. For operation with a resistive load, a positive value of the largest Lyapunov exponent λ_1 of 2.6 was calculated for the array voltage time series waveform shown in Fig. 11.

B. Frequency Spectrum

Figs. 12 and 13 show the normalized frequency spectrum of motor current for the three-level operation and the high

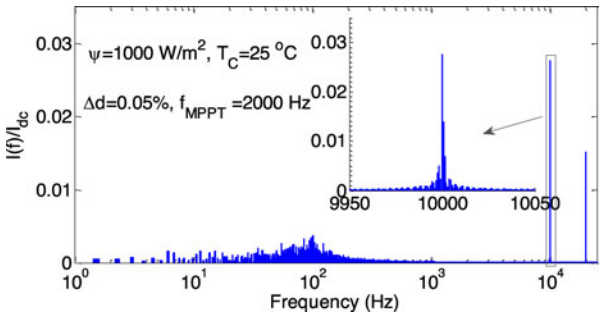

Fig. 13. Normalized frequency spectrum of motor current with operation at a high perturbation frequency.

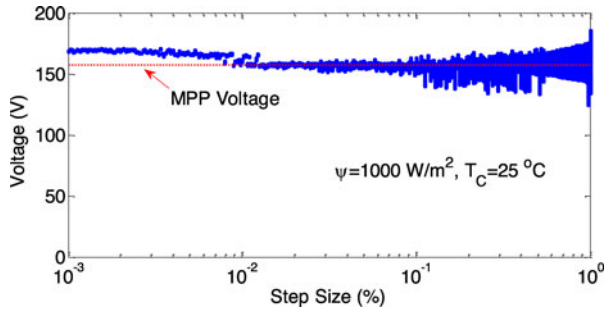

Fig. 14. Simulated array voltage/step size bifurcation diagram when the system is started with 75% duty ratio.

frequency operation, respectively. With three-level operation, system waveforms repeat every four perturbation samples as the middle level repeats twice. This produces frequency components at one-fourth and one-half of the perturbation frequency as shown in Fig. 12. The oscillation in the transient response to an MPPT perturbation results in frequency components around the natural frequency of the system which was calculated at about 100 Hz in [8]. There is also a frequency component at the switching frequency of the converter (10 kHz). The frequency spectrum of the motor current is made up of these components and their multiples. At high perturbation rates, the low frequency harmonics have lower amplitudes and a wider frequency spread compared to those with three-level operation, as shown in Fig. 13. The 2-kHz perturbation frequency results in frequency components at 1 and 2 kHz, but these are not significant due to the small step size used at high perturbation rates. Operation at 2 kHz also offers slightly lower harmonic amplitudes at the switching frequency and its side bands.

Usually, when comparing two MPPT algorithms the energy losses in the system are assumed to be the same for the same current level. When the frequency spectra of the current waveforms are not similar, this assumption needs to be reexamined. In the system under consideration, the frequency content of the motor current affects the ohmic losses of the converter and the motor, taking into consideration that the current through the switch during the on-time is the same as motor current (see Fig. 1). Ohmic losses are proportional to the square of the rms current which is higher than the average dc current when high frequency ripple is included. An ohmic loss increase factor (F_{OLI}) can be defined as

$$F_{\mathrm{OLI}} = \left(I_{\mathrm{rms}}^2 - I_{\mathrm{av}}^2\right)/I_{\mathrm{av}}^2. \tag{8}$$

A value of F_{OLI} of about 0.04% is calculated when operating at the high perturbation frequency compared to 0.15% at three-level operation. This means that at high perturbation rates there is a smaller increase in ohmic losses when compared to the three-level operation case. In any case, the increase in ohmic losses in both cases is very small and may be assumed negligible.

IV. Choice of Algorithm Parameters

For three-level operation, the perturbation period must be chosen higher than the settling time of the system response to a single MPPT perturbation. The step size is then chosen so that low steady-state oscillations are achieved with good transient characteristics [7], [8], [18]. For high perturbation rate operation, the perturbation frequency can be set at its maximum possible value equal to the ADC rate of the array voltage and current. This will facilitate the control as the duty ratio will be updated at the same rate of the measured parameters. Once the perturbation frequency has been chosen, there remains only one parameter of the P&O algorithm to be selected: the step size at which the duty ratio of the MPPT converter is perturbed.

In this paper, we are proposing that the duty ratio/array voltage bifurcation diagram (see Fig. 14) should be calculated and used as a design tool for defining the appropriate step size of the P&O algorithm. The term "bifurcation" represents a qualitative change in system dynamics which occurs as a system parameter is varied [22]–[24]. The diagram in which the varying parameter is plotted against a sampled variable is referred to as a bifurcation diagram. Bifurcation diagrams give a global view of the effect of the bifurcation parameter on system performance and can thus be used to identify the appropriate range of that particular parameter during the design stage.

Herein, the duty ratio-array voltage bifurcation diagram is obtained by taking 300 samples of the steady-state array voltage at the perturbation rate (2 kHz) for each value of the step size. The 300 samples of the array voltage at each step size value are spread around the maximum power point voltage (157.6 V) in a chaotic pattern (see Fig. 14). At very low step sizes, the P&O algorithm is not able to track the MPP. Instead, the system runs at equilibrium points near the initial operating point. The tracking algorithm begins to work at about 0.01% step size. The optimum operating step size range is between 0.02% and 0.07%. In this range, the array voltage ripple is low and the tracking speed is high. Step sizes above 0.1% cause higher swings in the duty ratio around the MPP duty ratio and thus low tracking efficiency and undesired motor operation.

The aforementioned bifurcation diagram is calculated for an irradiance level of 1000 W/m^2. For lower irradiance levels, the optimum step sizes will be slightly higher so that the perturbation results in measurable change in array power. For this reason, a step size of 0.05% was chosen for the experimental system under consideration which is suitable for the full irradiance range experienced at the installation site. The earlier discussion

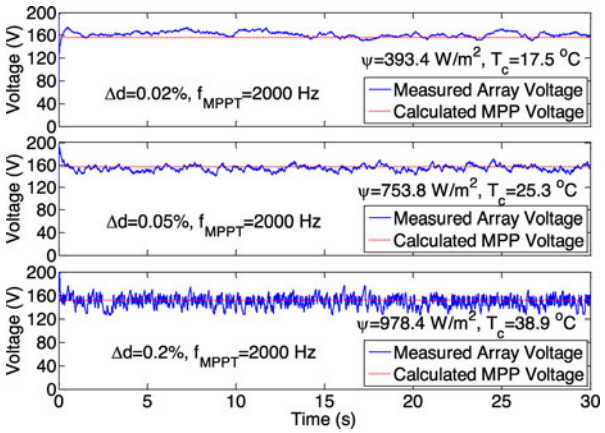

Fig. 15. Experimental results showing the influence of step size on the PV array voltage.

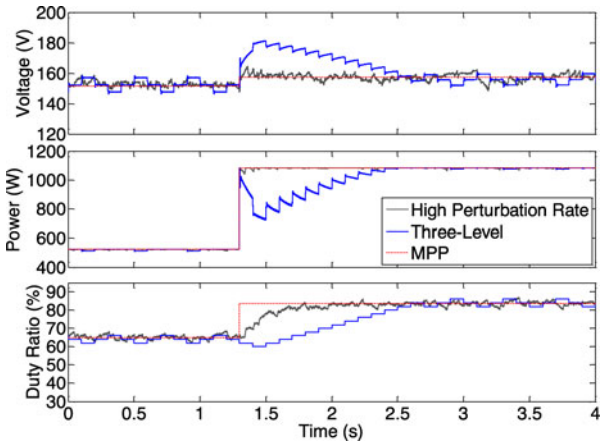

Fig. 16. Simulation results showing the response of the P&O algorithm to a step increase in solar irradiance.

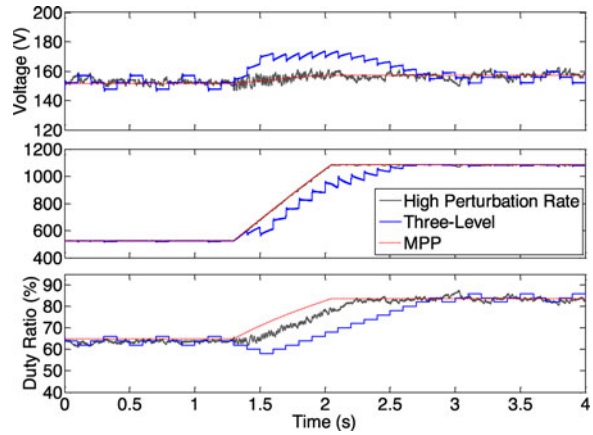

Fig. 17. Simulation results showing the response of the P&O algorithm to a ramp increase in solar irradiance.

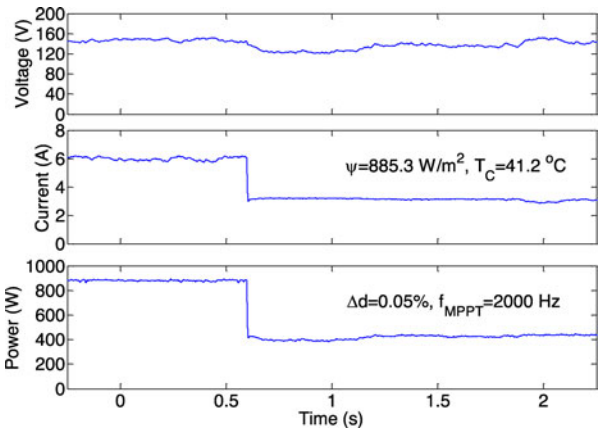

Fig. 18. Experimental results showing the array current, voltage, and power responses to a PV array branch disconnection.

regarding the choice of step size is verified by measuring the array voltage of the experimental system at three different step sizes (see Fig. 15). A larger step size (0.2% in Fig. 15) increases the algorithm speed compared to the speed of the system response resulting in faster recovery of the MPP but with a larger ripple magnitude in the array voltage and the other waveforms of the system, and vice versa. If the step size is low (0.02% in Fig. 15), the system may not respond to the variations in duty ratio and will spend long periods away from the MPP reducing the utilization efficiency of the algorithm.

V. Algorithm Confusion Due to Irradiance Changes

The P&O algorithm may be confused during solar irradiance changes. The MPP recovery time depends on the rate and magnitude of the irradiance change, and on the step size and the perturbation rate of the algorithm [8]. At high perturbation rates, the fast transient response of the P&O algorithm results in faster recovery of the MPP compared to the three-level operation mode. For example, for a step change in solar irradiance from 500 to 1000 W/m^2, the P&O algorithm reaches the new MPP in less than 1 s despite being confused many times by system dynamics (see Fig. 16). In fact, the continuous changes in the perturbation direction caused by system dynamics do not allow the algorithm to continue in the wrong perturbation direction for any length of time. With three-level operation, the response of the algorithm to the same step irradiance increase is much slower (see Fig. 16). The duty ratio remains at values lower than the new optimum for a longer period. The PV array, therefore, operates at voltages higher than the MPP voltage, reducing the energy utilization efficiency of the system.

Similarly, for a ramp change in solar irradiance, a high perturbation rate offers faster recovery of the MPP. For example, if the irradiance increases from 500 to 1000 W/m^2 in 0.75 s (see Fig. 17) the algorithm takes about 0.6 s to recover the MPP when operated at a low perturbation rate of 10 Hz. Using a 2-kHz perturbation rate, however, array voltage and power follow their optimum values almost instantaneously. The delay in duty ratio response to the irradiance change is due to the effect of the dc motor electrical time constant (L_a/R_a).

A step irradiance decrease can be experimentally emulated by disconnecting one of the two branches of the PV array while the system is running. This mimics a step decrease in solar irradiance to 50% of its original value. Fig. 18 shows how the algorithm moves the operating point to oscillate around the new MPP in a relatively short time (about 1 s) when an array branch

is disconnected at an irradiance level of 885.3 W/m^2 and a cell temperature of 41.2 °C. At low perturbation rates, the algorithm takes much longer to respond to a branch disconnection [8]. A step irradiance increase cannot be emulated in a similar way, as the two branches of the PV array are at different voltages before connection (the open-circuit voltage for the disconnected branch and the operating voltage for the one in service).

VI. Energy Utilization

At a particular set of algorithm parameters, the energy utilization efficiency of an MPPT algorithm depends on weather conditions and converter design in terms of noise immunity. Higher energy utilization efficiencies can be achieved at higher irradiance levels since the MPPT perturbations produce higher array power change magnitudes and consequently less algorithm confusion. At lower irradiance levels, the array power–voltage curve becomes flatter. In this case, the change in array power due to an algorithm perturbation becomes comparable to that caused by noise. This confuses the algorithm resulting in a lower energy utilization efficiency. Cell temperature changes have a less significant effect on the output power of the PV array and consequently reduced impact on the tracking efficiency of the P&O MPPT algorithm. Higher energy utilization efficiencies are expected for systems with better noise immunity as this reduces algorithm confusion.

The maximum energy utilization efficiency can be obtained with a noise-free system when irradiance is constant at a high level. This can be accomplished in simulation ignoring the effects of noise. For three-level operation, the maximum energy utilization efficiency of the system is calculated at 99.6%. This efficiency is achieved for three-level operation at 1000 W/m^2 solar irradiance and 25 °C cell temperature. In this case, the step size and perturbation rate of the P&O algorithm were set to their optimum values, calculated using the method detailed in [8]. Perhaps surprisingly, a higher energy utilization efficiency of 99.9% is obtained at the same weather conditions for operation with a high perturbation rate. Almost the same values of energy utilization efficiency are obtained when the simulation is run at a cell temperature of 60 °C (and 1000 W/m^2 solar irradiance) for both operation modes of the P&O algorithm.

The energy utilization efficiency for rapidly changing irradiance conditions varies depending on irradiance level and its rate of change. It was calculated for the 4-s duration shown in Fig. 16 which includes a step irradiance increase from 500 to 1000 W/m^2, for both low and high perturbation rate operation. A higher energy utilization efficiency of 99.8% was achieved with the high perturbation rate compared to 94.7% with three-level operation.

Slightly lower energy utilization efficiencies are obtained for practical systems where noise cannot be avoided. With high perturbation rates, algorithm operation is more sensitive to noise due to the use of lower step sizes at which noise may have a comparable effect to the MPPT perturbations. In this case, the degree to which the system benefits from operation at a high perturbation frequency depends on weather conditions.

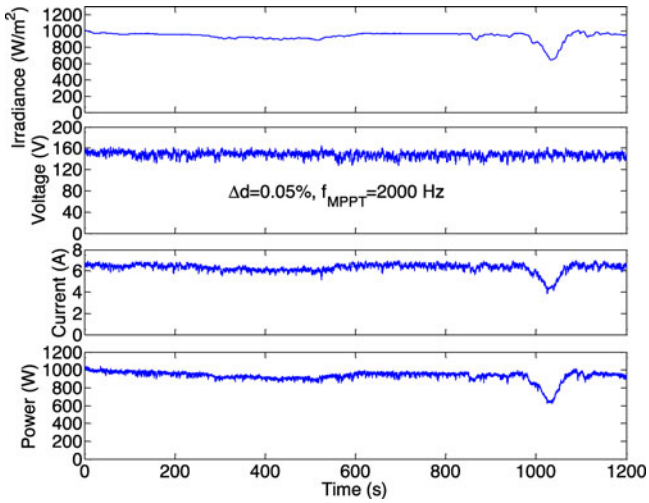

Fig. 19. Experimental system performance under slow changing irradiance.

A system operating at a high perturbation rate gives higher energy utilization efficiencies compared to one operating at three voltage levels at high irradiance values and rapidly changing irradiance and comparable energy utilization efficiencies at low irradiance levels.

For a site PV installation such as the one used in this investigation, the irradiance levels cannot be controlled as would be the case in simulation or under laboratory conditions. This precludes the use of MPPT algorithm evaluation standards that require measurements at specific controlled irradiance values and rates of change such as the European standard EN50530 [26]. For the experimental system under investigation, the energy utilization efficiency of the MPPT algorithm was calculated by dividing the integral of the PV array power by the integral of the maximum possible power output calculated at the same weather conditions [6], [8], [21]. This was calculated for a 20-min operation period and the test was repeated many times at different weather conditions. Results are shown to demonstrate the performance of the MPPT algorithm during periods of slow changing irradiance (see Fig. 19) and rapidly changing irradiance conditions (see Fig. 20). At slow changing irradiance, the energy utilization efficiency was about 98.8% for the 20-min period operating with a step size of 0.05% and a perturbation frequency of 2 kHz (see Fig. 19). At low step sizes, the P&O algorithm can be easily confused due to solar irradiance changes, system dynamics and/or noise. It recovers the correct perturbation direction quickly at high irradiance level where the change in duty ratio has a considerable effect on array power. At low irradiance levels, the system spends a longer time away from the MPP, as demonstrated in Fig. 20 during the period from 950 to 1200 s. This did not have a significant effect on the energy utilization efficiency since the maximum energy that can be drawn from the PV array is low under these conditions. The calculated energy utilization efficiency for the rapidly changing irradiance conditions shown in Fig. 20 is 96.6%.

For three-level operation, the algorithm is more confused at rapidly changing irradiance, as can be seen from the array

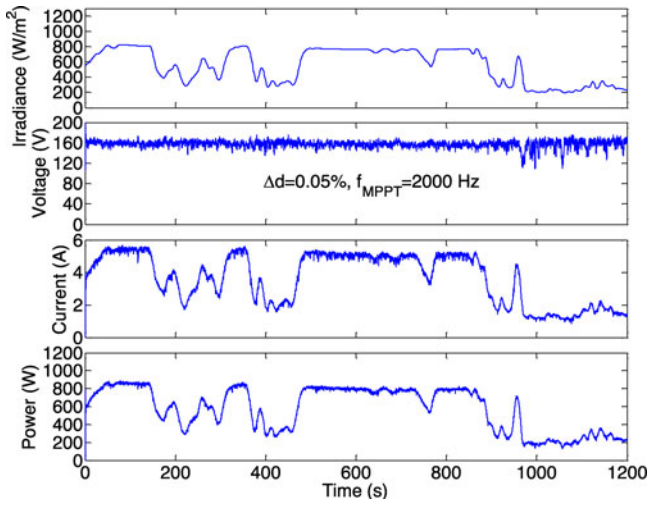

Fig. 20. Experimental system performance under rapidly changing irradiance.

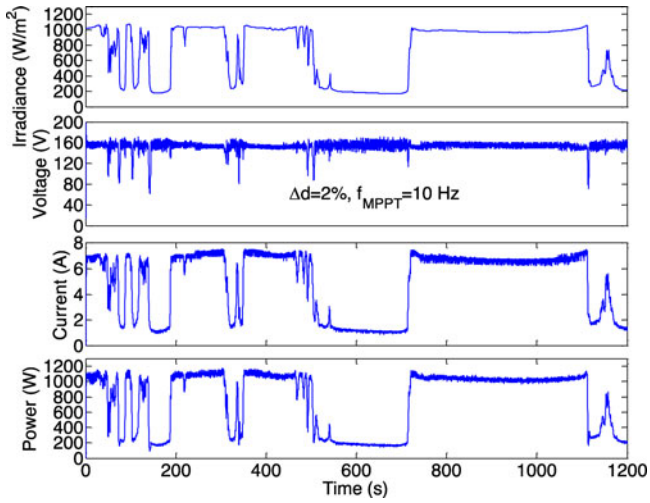

Fig. 21. Experimental system performance under rapidly changing irradiance, three-level operation.

voltage waveform in Fig. 21. This figure also shows wider variations in array voltage during low irradiance periods. However, the calculated overall energy utilization efficiency (97.9%) is higher than that obtained with high perturbation rate operation (see Fig. 20). This is due to the presence of long intervals of high-level irradiance shown in Fig. 21. Although the above tests cannot be repeated to give a direct comparison between the two modes of operation (as irradiance levels cannot be controlled in a site PV installation), they however give an indication of the energy utilization efficiencies at different weather conditions. It is also important here to mention that the power supplies used to emulate PV arrays cannot be used to evaluate the high perturbation rate case due to the relatively slow response of these emulators [27], [28].

Similarities and differences between three-level operation and operation at high perturbation rate of the P&O algorithm are summarized in Table I.

TABLE I
COMPARISON BETWEEN THREE-LEVEL OPERATION AND OPERATION AT A HIGH PERTURBATION RATE

	Three-level operation	**High perturbation rate**
Perturbation Parameter	$V_{\rm ref}$, $I_{\rm ref}$ or D	D only
Implementation cost	Low	Slightly higher
Steady-state fluctuations in array voltage	Three-level	Chaotic
Convergence speed	Parameter dependent	Faster
Electromagnetic interference	Parameter dependent	Less interference
Dependence of tracking efficiency on weather conditions	Dependent	Dependent
Tracking efficiencies for stationary weather conditions	High	Slightly higher
Tracking efficiencies for rapidly changing weather conditions	Slightly lower	High
Lower tracking efficiency at rapidly changing irradiance	Yes	Yes
Confusion due to noise	Yes	More confusion
Confusion due to irradiance changes	Yes	Less confusion
Confusion due to system dynamics	Yes	More confusion

VII. CONCLUSION

The paper presents a comprehensive analysis and evaluation of the performance of standalone PV systems employing the P&O MPPT algorithm when operating at a high perturbation frequency. Simulation and experimental results obtained from a 1080-Wp PV system are presented and the performance characteristics of the MPPT algorithm examined. A design criterion for selection of the algorithm parameters is proposed and the energy utilization efficiency of the experimental system calculated for both slow and rapidly changing weather conditions.

At high perturbation rates, the system is never allowed to reach a steady state. It often loses the local stability at the operating point and becomes very sensitive to the initial conditions producing chaotic system waveforms. However, the different waveforms are always bounded and the system is globally stable. When operated at a high perturbation frequency of 2 kHz (the ADC rate of the system), the P&O algorithm offered a faster transient response and a higher energy utilization efficiency during rapidly changing irradiance conditions when compared with conventional three-level operation. Similar energy utilization figures were obtained for both modes of operation during slowly changing weather conditions.

ACKNOWLEDGMENT

The authors would like to thank the staff at Narec and Dr. S. McDonald for the use of their PV arrays and for their valuable support. They would also like to thank Prof. S. Banerjee and Dr. D. Giaouris for their valuable comments and advice on nonlinear phenomena.

REFERENCES

[1] B. Subudhi and R. Pradhan, "A comparative study on maximum power point tracking techniques for photovoltaic power systems," *IEEE Trans. Sustain. Energy*, vol. 4, no. 1, pp. 89–98, Jan. 2013.

[2] M. A. de Brito, L. Galotto, Jr., L. P. Sampaio, G. de Azevedoe Melo, and C. A. Canesin, "Evaluation of the main MPPT techniques for photovoltaic applications," *IEEE Trans. Ind. Electron.*, vol. 60, no. 3, pp. 1156–1167, Mar. 2013.

[3] A. RezaReisi, M. H. Moradi, and S. Jamasb, "Classification and comparison of maximum power point tracking techniques for photovoltaic system: A review," *Renewable Sustain. Energy Rev.*, vol. 19, pp. 433–443, Mar. 2013.

[4] T. Esram and P. L. Chapman, "Comparison of photovoltaic array maximum power point tracking techniques," *IEEE Trans. Energy Convers.*, vol. 22, no. 2, pp. 439–449, Jun. 2007.

[5] K. Ishaque and Z. Salam, "A review of maximum power point tracking techniques of PV system for uniform insolation and partial shading condition," *Renewable Sustain. Energy Rev.*, vol. 19, pp. 475–488, Mar. 2013.

[6] M. A. Elgendy, B. Zahawi, and D. J. Atkinson, "Comparison of directly connected and constant voltage controlled photovoltaic pumping systems," *IEEE Trans. Sustain. Energy*, vol. 1, no. 3, pp. 184–192, Oct. 2010.

[7] S. B. Kjaer, "Evaluation of the "hill climbing' and the incremental conductance' maximum power point trackers for photovoltaic power systems," *IEEE Trans. Energy Convers.*, vol. 27, no. 4, pp. 922–929, Dec. 2012.

[8] M. A. Elgendy, B. Zahawi, and D. J. Atkinson, "Assessment of perturb and observe MPPT algorithm implementation techniques for PV pumping applications," *IEEE Trans. Sustain. Energy*, vol. 3, no. 1, pp. 21–33, Jan. 2012.

[9] A. Abdelsalam, S. Ahmed, A. Massoud, and P. Enjeti, "High performance adaptive perturb and observe MPPT technique for photovoltaic-based microgrids," *IEEE Trans. Power Electron.*, vol. 26, no. 4, pp. 1010–1021, Apr. 2011.

[10] L. Piegari and R. Rizzo, "Adaptive perturb and observe algorithm for photovoltaic maximum power point tracking," *IET Renew. Power Gen.*, vol. 4, no. 4, pp. 317–328, Jul. 2010.

[11] O. Wasynczuk, "Dynamic behavior of a class of photovoltaic power systems," *IEEE Trans. Power App. Syst.*, vol. PAS-102, no. 9, pp. 3031–3037, Sep. 1983.

[12] D. Sera, R. Teodorescu, J. Hantschel, and M. Knoll, "Optimized maximum power point tracker for fast-changing environmental conditions," *IEEE Trans. Ind. Electron.*, vol. 55, no. 7, pp. 2629–2637, Jul. 2008.

[13] A. Pandey, N. Dasgupta, and A. K. Mukerjee, "High-performance algorithms for drift avoidance and fast tracking in solar MPPT system," *IEEE Trans. Energy Convers.*, vol. 23, no. 2, pp. 681–689, Jun. 2008.

[14] M. Fortunato, A. Giustiniani, G. Petrone, G. Spagnuolo, and M. Vitelli, "Maximum power point tracking in a one-cycle-controlled single-stage photovoltaic inverter," *IEEE Trans. Ind. Electron.*, vol. 55, no. 7, pp. 2684–2693, Jul. 2008.

[15] H. Patel and V. Agarwal, "MPPT scheme for a PV-fed single-phase single-stage grid-connected inverter operating in CCM with only one current sensor," *IEEE Trans. Energy Convers.*, vol. 24, no. 1, pp. 256–263, Mar. 2009.

[16] M. E. Ropp and S. Gonzalez, "Development of a MATLAB/Simulink model of a single-phase grid-connected photovoltaic system," *IEEE Trans. Energy Convers.*, vol. 24, no. 1, pp. 195–202, Mar. 2009.

[17] E. Koutroulis, K. Kalaitzakis, and N. C. Voulgaris, "Development of a microcontroller-based, photovoltaic maximum power point tracking control system," *IEEE Trans. Power Electron.*, vol. 16, no. 1, pp. 46–54, Jan. 2001.

[18] N. Femia, G. Petrone, G. Spagnuolo, and M. Vitelli, "Optimization of perturb and observe maximum power point tracking method," *IEEE Trans. Power Electron.*, vol. 20, no. 4, pp. 963–973, Jul. 2005.

[19] R. Gules, J. D. P. Pacheco, H. L. Hey, and J. Imhoff, "A maximum power point tracking system with parallel connection for PV standalone applications," *IEEE Trans. Ind. Electron.*, vol. 55, no. 7, pp. 2674–2683, Jul. 2008.

[20] K. Lee and R. Kim, "An adaptive maximum power point tracking scheme based on a variable scaling factor for photovoltaic systems," *IEEE Trans. Energy Convers.*, vol. 27, no. 4, pp. 1002–1008, Dec. 2012.

[21] M. A. Elgendy, B. Zahawi, and D. J. Atkinson, "Dynamic behaviour of hill-climbing MPPT algorithms at low perturbation rates," in *Proc. IET Conf. Renew. Power Gen.*, Edinburgh, U.K., Sep. 2011, pp. 1–6.

[22] C. K. Tse, *Complex Behavior of Switching Power Converters*. Boca Raton, FL, USA: CRC Press, 2003.

[23] M. Lakshmanan and S. Rajaseekar, *Nonlinear Dynamics: Integrability, Chaos and Patterns*. Berlin, Germany: Springer-Verlag, 2003.

[24] D. C. Hamill, S. Banerjee, and G. C. Verghese, *Nonlinear Phenomena in Power Electronics; Attractors, Bifurcations, Chaos, and Nonlinear Control*. Hoboken, NJ, USA: Wiley, 2001.

[25] M. T. Rosenstein, J. J. Collins, and C. J. Deluca, "A practical method for calculating largest Lyapunov exponents from small data sets," *Physica D: Nonlinear Phenom.*, vol. 65, nos. 1/2, pp. 117–134, May 1993.

[26] BS EN 50530:2010+A1:2013, Overall Efficiency of Grid Connected Photovoltaic Inverters, BSI Standards Publication, 2013.

[27] H. Matsukawa, K. Koshiishi, H. Koizumi, K. Kurokawa, M. Hamada, and L. Bo, "Dynamic evaluation of maximum power point tracking operation with PV array simulator," *Solar Energy Mater. Solar Cells*, vol. 75, no. 3/4, pp. 537–546, Feb. 2003.

[28] S. H. Lloyd, G. A. Smith, and D. G. Infield, "Design and construction of a modular electronic photo-voltaic simulator," in *Proc. 8th Int. Conf. Power Electron. Variable Speed Drives*, London, U.K., Sep. 2000, vol. 475, pp. 120–123.

Mohammed A. Elgendy was born in Behera, Egypt, in 1974. He received the B.Sc. degree from Menoufia University, Menufia, Egypt, in 1997; the M.Sc. degree from Ain Shams University, Cairo, Egypt, in 2003; and the Ph.D. degree from Newcastle University, Tyne and Wear, U.K., in 2010, all in electrical engineering.

From June 1998 to May 2006, he was a Research Assistant at the New and Renewable Energy Department, Desert Research Centre, Cairo. He is currently a Research Associate at the School of Electrical and Electronic Engineering, Newcastle University. His research focus is on control of power electronic converters for photovoltaic systems and other renewable generation schemes.

Bashar Zahawi (M'96–SM'04) received the B.Sc. and Ph.D. degrees in electrical and electronic engineering from Newcastle University, Tyne and Wear, U.K., in 1983 and 1988, respectively.

From 1988 to 1993, he was a Design Engineer with a U.K. manufacturer of large variable speed drives and other power conversion equipment. In 1994, he was appointed as a Lecturer in Electrical Engineering at the University of Manchester, England. From 2003 to 2014, he was a Senior Lecturer at the School of Electrical and Electronic Engineering, Newcastle University. In 2014, he joined the faculty of the Department of Electrical and Computer Engineering, Khalifa University, Abu Dhabi, UAE, where he holds the position of Professor of Electrical Power Engineering. His research interests include power conversion and the application of nonlinear dynamical methods to electrical circuits and systems.

Dr. Zahawi is a recipient of the Crompton Premium awarded by the Institution of Electrical Engineers and the Denny Medal awarded by the Institute of Marine Engineering, Science, and Technology. He is a Chartered Electrical Engineer.

David J. Atkinson received the B.Sc. degree in electrical and electronic engineering from Sunderland Polytechnic, Sunderland, U.K., in 1978, and the Ph.D. degree from Newcastle University, Tyne and Wear, U.K., in 1991.

He is currently a Senior Lecturer in the Power Electronics, Drives, and Machines Research Group, School of Electrical and Electronic Engineering, Newcastle University. He joined the Newcastle University in 1987 after 17 years in industry with NEI Reyrolle Ltd., Hebburn, England, and British Gas Corporation, Cramlington, England. His research interests include the control of power electronics systems including electric drives and converters.

Dr. Atkinson is a Chartered Electrical Engineer and a recipient of the Power Premium awarded by the Institution of Electrical Engineers.